Optofluidic Characterization of Nanoporous Membranes

ARTICLE *in* LANGMUIR · FEBRUARY 2013

Impact Factor: 4.46 · DOI: 10.1021/la304869y · Source: PubMed

Langmuir

Article

pubs.acs.org/Langmuir

Optofluidic Characterization of Nanoporous Membranes

Raúl Urteaga,*[,†] Leandro N. Acquaroli,[†] Roberto R. Koropecki,[†] Abel Santos,[‡] María Alba,[‡] Josep Pallarès,[‡] Lluís F. Marsal,[‡] and Claudio L. A. Berli[†]

[†]INTEC, Universidad Nacional del Litoral-CONICET, Güemes 3450, 3000 Santa Fe, Argentina

[‡]Departament d'Enginyeria Electrònica, Elèctrica i Automàtica, Universitat Rovira i Virgili, Avda. Països Catalans 26, 43007 Tarragona, Spain

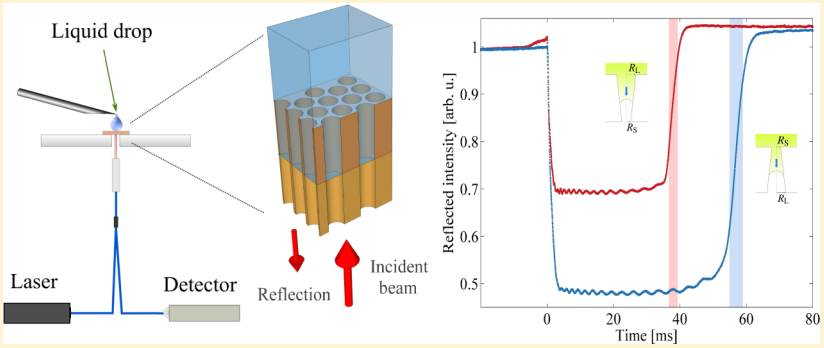

ABSTRACT: An optofluidic method that accurately identifies the internal geometry of nanochannel arrays is presented. It is based on the dynamics of capillary-driven fluid imbibition, which is followed by laser interferometry. Conical nanochannel arrays in anodized alumina are investigated, which present an asymmetry of the filling times measured from different sides of the membrane. It is demonstrated by theory and experiments that the capillary filling asymmetry only depends on the ratio H of the inlet to outlet pore radii and that the ratio of filling times vary closely as $H^{7/3}$. Besides, the capillary filling of conical channels exhibits striking results in comparison to the corresponding cylindrical channels. Apart from these novel results in nanoscale fluid dynamics, the whole method discussed here serves as a characterization technique for nanoporous membranes.

INTRODUCTION

The integration of optics and microfluidics is a rapidly developing field of research,[1] and applications are continuously growing, for example, in chemical and biological sensing.[2] Many of these applications involve arrays of nanochannels or nanoholes, which are employed in different areas such as nanofluidic concentration,[3] DNA manipulation,[4] and virus detection,[5] to mention a few. For these purposes, and with the evolution of microfabrication techniques, regular structures with uniform pore-size distributions are currently being produced in different substrates. However, the detailed internal structure of nanochannels is still inaccessible to ordinary techniques used in nanotechnology laboratories, without destroying the sample.

In this framework, a recent paper[6] discussed the implementation of an optical technique to investigate the dynamics of capillary-driven fluid imbibition in nanoporous substrates. The method can be used either as a nanofluidic sensor or to characterize the internal structure of nanoporous matrices in a nondestructive manner. The latter possibility is exploited in this work, where the geometry of nanoporous anodic alumina membranes (NAAMs) is elucidated, showing a clear advantage in relation to classical techniques, such as electron microscopy. The method takes advantage of the fact that nanochannel arrays permit the flow of liquids through them and, at the same time, behave as effective media when interact with visible electromagnetic waves. Thus, we use laser interferometry with submillisecond resolution to follow the dynamics of capillary-driven fluid imbibition into the substrates.[6] The method deals with reflectance interference and hence can be regarded as a variation of the well-known Fabry–Pérot interferometry, which has been also used to study nanoscale fluid dynamics.[7]

Nanoporous membranes are studied by measuring the imbibition rate of sessile drops on both sides of the membrane. It is found that the times required to fill the pores present a strong asymmetry depending on which side of the membrane is wet. This behavior has been previously reported in NAAMs,[8] though associated with another cause: the presence of different pore structures on each side of the membrane. The substrates considered here contain a well-ordered array of straight nanopores with very large aspect ratios and conical geometry. In fact, we show that the asymmetric filling closely depends on the ratio H of the inlet to outlet pore radii. Moreover, we show by theory and experiments that the relative filling times vary as $H^{7/3}$. The geometry of nanochannels in NAAMs is thus

Received: December 10, 2012
Revised: February 1, 2013
Published: February 1, 2013

   dx.doi.org/10.1021/la304869y | *Langmuir* 2013, 29, 2784–2789

elucidated, showing a clear advantage in relation to classical techniques, such as electron microscopy. It is worthwhile to stress that the fluid imbibition we are dealing with is driven by capillary forces, in contrast to the experiments of equilibrium wetting and capillary condensation carried out with NAAMs,[9] which may be also sensitive to pore structure and morphology.[10,11]

The paper is organized as follows: the next section presents the fabrication of NAAMs and the setup of the optofluidic experiment. Then the theoretical section includes the basis of optical measurements and the equations to describe capillary flow in conical channels. Finally, the experimental results are discussed, and the main conclusions are outlined.

MATERIALS AND METHODS

Nanoporous Membranes Preparation. NAAMs were fabricated by the two-step anodization process.[12−16] Before anodization takes place, aluminum (Al) foils were electropolished under constant potential in a mixture of perchloric acid ($HClO_4$) and ethanol (EtOH). After this, the first electrochemical anodization was performed by applying direct voltage to the electropolished Al films in acidic solutions of sulfuric acid (H_2SO_4) and oxalic acid ($H_2C_2O_4$). Then, the aluminum oxide film with disordered pores was dissolved by wet chemical etching using a mixture of phosphoric acid (H_3PO_4) and chromic acid (H_2CrO_4). Then, the second anodization step was started under the same anodization conditions and carried out until the NAAMs reached the desired thicknesses (about 75 μm). Thereafter, the remaining aluminum substrate was removed from the bottom side by wet chemical etching in a saturated solution of cupric chloride and hydrochloric acid ($CuCl_2$/HCl). Subsequently, a pore opening process was performed by wet chemical etching under current control.[15,16] In order to modify the porosity of the NAAMs (i.e., the pore diameter), a pore widening process was performed by wet chemical etching in a phosphoric acid solution. Thereby, a hexagonally distributed pore array is obtained with pore diameter between 20 and 50 nm and center-to-center pore distance ranging from 50 to 100 nm. A slight reduction in pore diameter is obtained across the membrane (about 20% in 75 μm), resulting in a bundle of cones with a very small angle (about 0.007°).

After the fabrication process, both sides of the NAAMs were inspected by SEM (ESEM FEI Quanta 600); typical images are included in Figure 1b,c. The average values of the pore radius, the center-to-center pore distance, and the membrane thickness (i.e., pore length) were calculated from SEM image analysis. In order to reduce the uncertainty in the data, the pore diameter and the center-to-center pore distance of the top and bottom side were measured at four different areas of each NAAM (separated each other by about 0.5 mm). The membrane thickness was estimated at eight different points of the cross-section side of each NAAM.

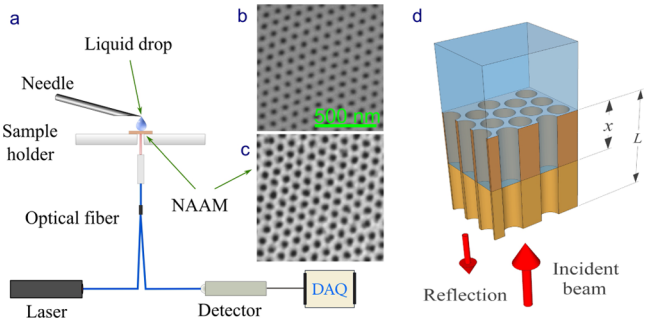

Figure 1. (a) Diagram of the experimental setup. A liquid drop released from a needle reaches the NAAM, and the liquid penetrates into the porous membrane by capillary forces. A monochromatic laser diode (λ = 980 nm) is focused on the porous membrane from the rear, and the evolution of the laser reflectance is measured at 48 kHz. (b, c) SEM images of each side of a typical NAAM, for which image analysis yields average values of 28 and 34 nm for the top and bottom views, respectively. (d) Schematic representation of the nanochannels array with the imbibing fluid and the coordinate systems used in calculations.

Measurement System. The experiment setup is similar to that reported in ref 6. We measure light reflectance as a function of time, after a liquid drop released from a needle impinges over the NAAMs, as shown in Figure 1a. A laser beam (980 nm) is focused onto a NAAM by employing optical fibers. The light reflected from the NAAM (at low angle, 5°) is measured by using a photodetector with linear response. Data where recorded at 48 kHz with a 14 bits computer controlled data acquisition card. The sample holder (Figure 1a) has a hole that allows light to interact only with the porous membrane. This also ensures that pores are open to the atmosphere at both ends.

THEORY

Fluid Dynamic Model. Given the well-ordered array of pores in anodized alumina (Figure 1), the membrane can be considered as an assembly of straight nanochannels aligned in the flow direction, all of them with the same length and pore radius. Under these conditions, and taking into account that pores are not interconnected, the velocity at which the liquid invades the membrane is that of the capillary-driven flow in each single pore. Thus, the fluid dynamics of a single capillary can be used to model the imbibition of the whole nanopore membrane, as a first approximation (a narrow distribution of pore radii may be present).

Capillary filling of nanochannels due to Laplace pressure is described in the framework of continuum fluid mechanics. Incompressible fluids of viscosity μ and surface tension σ are considered, which form a meniscus at the liquid−gas interface with a contact angle θ. In capillaries of large aspect ratios, the steady-state balance of capillary and viscous forces (pore ends are open and gravity effects are neglected) leads to the following expression for the velocity of the meniscus

$$\frac{dx}{dt} = \frac{\sigma \cos\theta}{4\mu R(x)^3 \int_0^x R(x')^{-4}\, dx'} \quad (1)$$

where $R(x)$ is the axially dependent channel radius. This equation is normally the starting point to analyze capillary flow in tubes of nonuniform cross section.[17−19] In the trivial case of cylindrical capillaries of uniform radius R and length L, the integration of eq 1 yields

$$\bar{x}^2 = t/t_F \quad (2)$$

which is the classical Lucas−Washburn equation[20,21] for the dimensionless distance $\bar{x} = x/L$ traveled by the fluid in the axial direction of the capillary, as a function of time t. In eq 2, $t_F = 2\mu L^2/(R\sigma \cos\theta)$ is the characteristic filling time.

Now we consider the imbibition of nanochannels with a monotonic variation of the cross-sectional size along the x-direction: more precisely, axisymmetric conical channels with the smallest radius R_S at one end, and the largest radius R_L at the other end. Given that $L/R_L \sim 10^3$ in NAAMs, the opening angle of the cone is very small, $\alpha \approx (R_L - R_S)/L \sim 10^{-4}$, and hence, the assumption of one-dimensional flow is accurate. Further, as we study flow imbibition from both sides of the membrane, the fluid dynamics is described in both directions, when the pore radius opens in the direction of the flow and vice versa. If the fluid enters through the narrowest end (R_S at x =

dx.doi.org/10.1021/la304869y | Langmuir 2013, 29, 2784−2789

0) and flows toward the widest end (R_L at $x = L$), the radius changes along the channel as $R(x) = R_S + \alpha x$. Solving eq 1 with this function yields

$$\frac{1}{6}(H-1)^2\bar{x}^4 + \frac{2}{3}(H-1)\bar{x}^3 + \bar{x}^2 = t/t_{F,S} \quad (3)$$

where $H = R_L/R_S$ and $t_{F,S} = 2\mu L^2/(R_S\sigma\cos\theta)$, which represents the filling time of a cylindrical channel with uniform radius R_S.

On the other hand, if the fluid enters through the largest end (R_L at $x = 0$) and flows toward the smallest end (R_S at $x = L$), the pore radius shrinks in the direction of the flow as $R(x) = R_L - \alpha x$. Then solving eq 1 with this function results in

$$\frac{1}{6}(H^{-1}-1)^2\bar{x}^4 + \frac{2}{3}(H^{-1}-1)\bar{x}^3 + \bar{x}^2 = t/t_{F,L} \quad (4)$$

where $t_{F,L} = 2\mu L^2/(R_L\sigma\cos\theta)$ represents the filling time of a cylindrical channel with uniform radius R_L. Equations 3 and 4 indicate that the kinematics of fluid imbibition no longer satisfies the scaling of eq 2, except at very short times where $\bar{x} \ll 1$. When the meniscus advance into the conical geometry, the fact that viscous force varies as $R(x)^{-2}$ while capillary force varies as $R(x)^{-1}$ yields the polynomial relationships. Consistently, Lucas–Washburn law is recovered when $H = 1$. It is relevant to note that eqs 3 and 4 have not been reported before. However, an expression analogous to eq 3 has been previously derived for semi-infinite opening cones.[18]

For a given fluid, the relation between the time required to fill the capillary in the opening cone direction [$t_O = t(\bar{x}=1)$ in eq 3] and that in the closing cone direction [$t_C = t(\bar{x}=1)$ in eq 4] is completely defined by the ratio $H = R_L/R_S$. In fact, taking the ratio of eqs 3 and 4 with $\bar{x} = 1$ (complete filling) yields the following expression:

$$\frac{t_O}{t_C} = \frac{H^5 + 2H^4 + 3H^3}{3H^2 + 2H + 1} \approx H^{7/3} \quad (5)$$

The second equality, which involves a simple power of H, is empirical and valid for a wide range of H values around 1. Equation 5 predicts a strong asymmetry of the filling times from different sides of the membrane. In particular, the filling process is faster when the cone closes in the direction of the flow. It is shown below that, even if nanochannels are very slim, and its opening angles are very small, the effect can be measured by combining fluidics and optics.

Optical Model. Since the laser wavelength (980 nm) is much greater than pore dimensions, the membrane can be considered as an effective medium whose refractive index can be calculated by using different approaches depending on its specific morphology.[22] The total reflected intensity depends upon the contribution of the reflection from the two interfaces of the porous membrane and the moving interface of the liquid inside the NAAM (Figure 1d). In particular, the reflection at the moving liquid–air interface is small because the refractive index contrast is smaller than in the other two interfaces and because the moving interface is not perfectly flat due to small filling differences in individual channels.[23] Therefore, the measured intensity is determined by the interference of light reflected from the two fixed interfaces. The interference will be constructive when the phase shift $\Delta\varphi$ is a multiple of 2π and destructive when $\Delta\varphi$ is an odd multiple of π. Taking into account the phase shift at the first interface, the total phase shift will be

$$\Delta\varphi = \pi + 4\pi e_0/\lambda \quad (6)$$

where $e_0 = \int_0^L n_{eff}(x)\,dx$ is the optical path thickness of the membrane, and $n_{eff}(x)$ is the effective refractive index. As the liquid penetrates into the porous layer, $n_{eff}(x)$ increases, so does the optical path, and the reflectance reaches extremes every time e_0 is a multiple of $\lambda/4$.

The effective refractive index can be estimated by using the simple Looyenga–Landau–Lifshitz approximation,[24] which for a bundle of cylindrical-like pores simply results in $n_{eff} = \Sigma_i n_i f_i$, where n_i and f_i are, respectively, the refractive index and volume fraction of each component: $i = 1$, alumina; $i = 2$, liquid; $i = 3$, air. Therefore the optical path can be calculated as

$$e_0 = \int_0^L n_1[1 - p(x)]\,dx + \int_0^x n_2 p(x')\,dx' + \int_x^L n_3 p(x')\,dx' \quad (7)$$

where $p(x) = \pi R(x)^2\delta$ is the local membrane porosity, δ being the pores surface density. By differentiating eq 7 with respect to x one has

$$de_0/dx = (n_2 - n_3)\pi R(x)^2\delta \quad (8)$$

In the case of conical nanochannels, when the fluid enters through the narrowest end and flows toward the widest end, $R(x) = R_S + \alpha x$. Then integrating eq 8 with this function yields an explicit relationship between the optical thickness and the relative position of the liquid front:

$$e_0(\bar{x}) = (n_2 - n_3)\pi {R_S}^2\delta L\left[\bar{x} + (H-1)\bar{x}^2 + \frac{1}{3}(H-1)^2\bar{x}^3\right] \quad (9)$$

In addition, when the fluid enters through the widest end and flows toward the narrowest end, $R(x) = R_L - \alpha x$, and the integration of eq 8 yields

$$e_0(\bar{x}) = (n_2 - n_3)\pi {R_L}^2\delta L\left[\bar{x} + (H^{-1}-1)\bar{x}^2 + \frac{1}{3}(H^{-1}-1)^2\bar{x}^3\right] \quad (10)$$

Therefore, using these expressions in eq 6 allows one to associate the extremes of the measured light reflectance to the instantaneous position of the moving liquid front, taking into account the pore radius variation across the membrane. It is worth noting that if $H = 1$, one recovers the lineal relation $\Delta\varphi(x)$ used in our previous work for cylindrical nanochannels.[6]

RESULTS AND DISCUSSION

Figure 2 presents the normalized reflectance of a 75 μm thick NAAM when it is filled with 2-propanol at room temperature. As pores in NAAMs act as open-end nanochannels, the filling dynamics could be measured from both sides. In both cases, at the beginning of the experiment, when the liquid reaches the surface, the reflectance decreases steeply due to the sudden change in the refractive index contrast at the upper interface. Then small oscillations are observed as a result of the interference related to the change of e_0 with fluid imbibition (this particular aspect is discussed in Figure 4). When pores are completely filled, the reflectance grows again due to the increases of the refractive index contrast at the lower interface. The second intensity step is less abrupt than the first one

dx.doi.org/10.1021/la304869y | Langmuir 2013, 29, 2784–2789

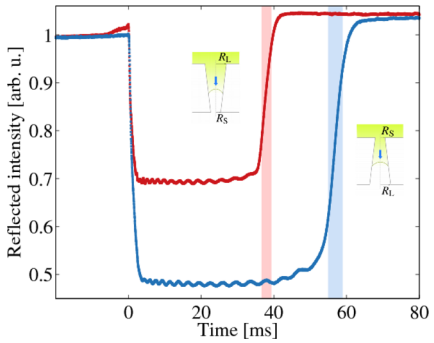

Figure 2. Normalized reflectance measured from both sides of the same NAAM, when a 2-propanol drop is release over the membrane. The insets show schematically the flow direction of each measurement. In both cases, at zero time the liquid reaches the porous layer and the reflectance decreases. When the liquid completely fill the pores, the reflectance grows again. The ratio $t_O/t_C \approx 1.49$ reasonably coincides with $H^{7/3} \approx 1.57$, with pore radii values estimated from SEM image analysis ($R_S \approx 28$ nm and $R_L \approx 34$ nm; Figure 1b,c).

because not all the pores are filled at exactly the same time, taking into account that a narrow distribution of pore sizes is present. Accordingly, the filling times in NAAMs, in one direction or another, have a narrow range (shaded areas in Figure 2) rather than definite values. In any case, the filling times corresponding to the imbibition from different sides of the membrane are quite distinctive, despite the relatively slight variation in pore diameter across the membrane (about 20%). Approximate values in this example are $t_C \approx 39$ ms and $t_O \approx 58$ ms.

Interestingly, these filling time values allow one to determine the radii R_S and R_L by solving the set of eqs 3 and 4 with $\bar{x} = 1$, provided the NAAM thickness and the fluid properties σ, θ, and μ are known (in particular, perfect wetting is assumed in calculations, i.e., $\cos\theta = 1$). Figure 3 presents a graphic solution of this problem. The shaded zones A and B represent the combination of radii that yield the times t_C and t_O, respectively, for $L = 75$ μm and 2-propanol properties. Regions A and B are zones instead of lines due to the narrow dispersion of filling times. Furthermore, the combination of radii that simultaneously gives the right values of t_O and t_C (overlapping of zones A and B) coincide with those estimated from SEM image analysis (Figure 1b,c).

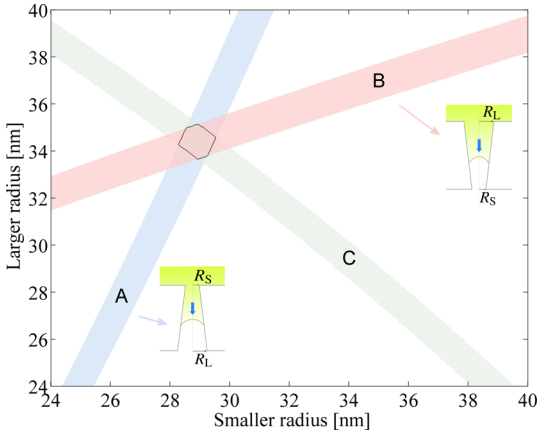

Figure 3. Determination of the pore sizes of the NAAM. Zones A and B represents the combination of pore radii that reproduce the measured filling times in both directions. Zone C comes from the optical model and represents the combination of radii that reproduces the NAAM porosity. Radii values estimated from SEM lie inside the overlapped area.

The corresponding R_S and R_L values (about 29 and 34 nm, respectively; Figure3) are also in agreement with those obtained from SEM. However, concerning the characterization of the membrane, this optofluidic technique presents some advantages in relation to microscopy. In fact, quantification of objects size from image analysis of SEM requires a crucial step that consists of defining a threshold, which is normally done by gray levels. The cut off value for pixel intensity may be rather arbitrary; thus, pore radii are difficult to determine accurately. The relative errors take relevance when pores sizes are about a few nanometers. In contrast, the optofluidic technique we are discussing here allows one to precisely determine both radii, by measuring the filling times on each side of the membrane.

In addition, the total number of oscillations in each experiment of Figure 2 allows one to determine the optical thickness variation, and hence the average refractive index of the membrane for a given physical thickness. Then the average membrane porosity is calculated by using an effective medium model,[22] which results in 34% for the NAAM used in Figure 2. Besides, as the center-to-center distance is accurately determined from SEM image analysis (it does not depend on contrast adjusting), one can estimate the combination of radii that reproduces the NAAM porosity. This is represented by zone C in Figure 3 (the solution is not a line because of the small uncertainties in the determination of the total number of oscillations). The intersection of zone C (optical model) with the overlapping of zones A and B (fluid dynamic model) is a successful cross-check of results.

Finally, we discuss the imbibition dynamics. As stated above, between two consecutive extremes of the reflectance oscillations reported in Figure 2, the optical thickness changes a quarter wave. Thus, as the geometry of the channels is in principle known, each extreme of the oscillations is related to the instantaneous position of the liquid front through eqs 9 and 10. Figure 4 shows the normalized squared position ($\bar{x}^2$) of the interface as a function of time, when the drop is released from both sides of the NAAM (data points). The insets schematically show the flow direction for each measurement. Full lines in Figure 4 are the theoretical predictions for each case, according to eqs 3 and 4. A reasonable agreement between experiments

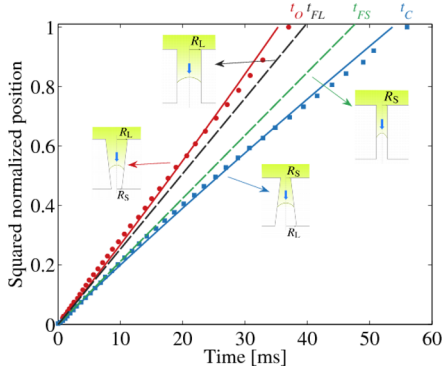

Figure 4. Filling dynamics of 2-propanol from both sides of the membrane (symbols) in the direction shown in the insets. Full lines are the theoretical predictions according to eqs 3 and 4. Dashed lines are the expected filling dynamics for cylindrical channels with radii R_S and R_L, after eq 2 (Lucas–Washburn regime).

dx.doi.org/10.1021/la304869y | Langmuir 2013, 29, 2784–2789

and the optofluidic model is observed. Additionally, dashes lines are the expected dynamics of capillary filling of cylinders of radii R_S and R_L, according to eq 2.

It is worth noting that the filling time for the opening cone (t_O) is larger than $t_{F,S}$, while the filling time for the closing cone (t_C) is shorter than $t_{F,L}$. This rather counterintuitive behavior can be understood as follows. In a cylindrical capillary, when the fluid advances along the channel, the driving force (capillary pressure, $\sigma \cos \theta/R$) keeps constant, whereas the hydrodynamic resistance increases with the wetted length. In a conical capillary that opens in the flow direction, the capillary pressure progressively decreases with $R(x)$. At the same time, the hydrodynamic resistance increases with x, but at a rate that is slower than that in a cylinder with uniform radius R_S. In a conical capillary that shrinks along the direction of the flow, the capillary pressure increases as $R(x)$ decreases. The hydrodynamic resistance also increases, but at a rate that is larger than that in a cylinder of radius R_L. The overall result is a strong asymmetry of the filling times, depending on the flow direction in the membrane. This behavior has been also predicted by model simulation of capillary imbibition of porous substrates consisting of two layers with different permeabilities: filling times are lower from large opening to small opening pores, and vice versa.[25]

The asymmetry discussed here may sound in apparent contradiction with the fact that low Reynolds number flows of Newtonian fluids are essentially reversible, and hence, the hydrodynamic resistance of an arbitrary channel must be the same in both flow directions.[26,27] In this regard, it should be noted that we are dealing with fluid invasion into the solid geometry, where the fluid undergoes different hydrodynamic resistance depending on which side of the conical channel is invading. Precisely, for nonhomogeneous channels, the isotropic processes are filling and emptying from the same inlet: changing the sign of pressure difference produces an isotropic flow reversion. These fundamental aspects also open new potential applications for asymmetric nanopores in microfluidics and optofluidics, where rectification properties are highly desirable.

CONCLUSIONS AND PERSPECTIVES

The present work involves two main aspects: first we present an optofluidic method to investigate the dynamics of flow imbibitions in nanoporous substrates, which accurately identifies the internal geometry of nanochannels in a non-destructive manner. This is an advantage in relation to scanning electron microscopy, and thus, the method is of special interest for the characterization of nanoporous matrices.

More precisely, if both the geometry and the arrangement of the nanochannels are specified, one may predict the curves $x(t)$ and $e_0(t)$ to be obtained in an imbibition experiment with a given fluid. This possibility may be designated direct calculation. In contrast, a more challenging problem is the inverse calculation, i.e., determining the internal characteristics of nanoporous substrates, that is, completely unknown functions $R(x)$, from the curve of raw reflectance data. The implementation of this task requires further efforts, and it is currently under research.

The second aspect concerns fundamentals. It is shown that conical nanochannels present a clear anisotropy of capillary filling times, even if they are extremely slim. We theoretically demonstrate that the asymmetry only depends on the ratio H of the inlet to outlet pore radii and that the ratio of filling times follows the power law $H^{7/3}$. Besides, the capillary filling of conical channels exhibits striking results in comparison to the corresponding cylindrical channels. These are novel results in nanoscale fluid dynamics, which also open new potential applications for nanochannel arrays, for instance, in the attractive fields of nanofiltration and flow rectification.

AUTHOR INFORMATION

Corresponding Author

*E-mail: urteagar@santafe-conicet.gov.ar.

Notes

The authors declare no competing financial interest.

ACKNOWLEDGMENTS

The authors acknowledge the financial support from the CONICET and the Universidad Nacional del Litoral (FIQ), Argentina, the Spanish Ministry of Economy and Competitiveness (MINECO) under grant number TEC2012-34397, and the Catalan authority under project 2009 SGR 549. We also acknowledge the technical support of Ramón Saavedra and Raquel Urteaga.

REFERENCES

(1) Psaltis, D.; Quake, S. R.; Yang, C. Developing optofluidic technology through the fusion of microfluidics and optics. *Nature* **2006**, *442*, 381−386.

(2) Fan, X.; White, I. M. Optofluidic microsystems for chemical and biological analysis. *Nat. Photonics* **2011**, *5*, 591−597.

(3) Escobedo, C.; Brolo, A. G.; Gordon, R.; Sinton, D. Optofluidic concentration: Plasmonic nanostructure as concentator and sensor. *Nano Lett.* **2012**, *12*, 1592−1596.

(4) Serey, X.; Mandal, S.; Chen, Y.-F.; Erickson, D. DNA transport and delivery in thermal gradients near optofluidic resonators. *Phys. Rev. Lett.* **2012**, *108*, 048102.

(5) Rai, V.; Hapuarachchi, H. C.; Ng, L. C.; Soh, S. H.; Leo, Y. S.; Toh, C.-S. Ultrasensitive cDNA detection of dengue virus RNA using electrochemical nanoporous membrane-based biosensor. *PLoS One* **2012**, *7*, e42346.

(6) Acquaroli, L. N.; Urteaga, R.; Berli, C. L. A.; Koropecki, R. R. Capillary filling in nanostructured porous silicon. *Langmuir* **2011**, *27*, 2067−2072.

(7) Van Delft, K. M.; Eijkel, J. C. T.; Mijatovic, D.; Druzhinina, T. S.; Rathgen, H.; Tas, N. R.; Van den Berg, A.; Mugele, F. Micromachined Fabry−Pérot interferometer with embedded nanochannels for nanoscale fluid dynamics. *Nano Lett.* **2007**, *7*, 345−350.

(8) Grzelakowski, C.; Ben Jazia, D.; Lebeau, B.; Vonna, L.; Dupuis, D.; Haidara, H. On the influence of pore structure on the free-imbibition of sessile drops into nanoporous substrates. *Langmuir* **2009**, *25*, 5855−5860.

(9) Alvine, K. J.; Shpyrko, O. G.; Pershan, P. S.; Shin, K.; Russell, T. P. Capillary filling of anodized alumina nanopore arrays. *Phys. Rev. Lett.* **2006**, *97*, 175503.

(10) Bruschi, L.; Mistura, G.; Liu, L.; Lee, W.; Gösele, U.; Coasne, B. Capillary condensation and evaporation in alumina nanopores with controlled modulations. *Langmuir* **2010**, *26*, 11894−11898.

(11) Casanova, F.; Chiang, C. E.; Ruminski, A. M.; Sailor, M. J.; Schuller, I. K. Controlling the role of nanopore morphology in capillary condensation. *Langmuir* **2012**, *28*, 6832−6838.

(12) Masuda, H.; Fukuda, K. Ordered metal nanohole arrays made by a two-step replication of honeycomb structures of anodic alumina. *Science* **1995**, *268*, 1466.

(13) Masuda, H.; Hasegwa, F.; Ono, S. Self-ordering of cell arrangement of anodic porous alumina formed in sulfuric acid solution. *J. Electrochem. Soc.* **1997**, *144*, L127−L130.

(14) Vojkuvka, L.; Marsal, L. F.; Ferré-Borrull, J.; Formentin, P.; Pallarés, J. Self-ordered porous alumina membranes with large lattice

constant fabricated by hard anodization. *Superlattices Microstruct.* **2008**, *44*, 577−582.
(15) Lillo, M.; Losic, D. Pore opening detection for controlled dissolution of barrier oxide layer and fabrication of nanoporous alumina with through-hole morphology. *J. Membr. Sci.* **2009**, *327*, 11−17.
(16) Losic, D.; Losic, D., Jr. Preparation of porous anodic alumina with periodically perforated pores. *Langmuir* **2009**, *25*, 5426−5431.
(17) Staples, T. L.; Shaffer, D. G. Wicking flow in irregular capillaries. *Colloids Surf. A* **2002**, *204*, 239−250.
(18) Reyssat, M.; Courbin, L.; Reyssat, E.; Stone, H. A. Imbibition in geometries with axial variations. *J. Fluid Mech.* **2008**, *615*, 335−344.
(19) Liou, W. W.; Peng, Y.; Parker, P. E. Analytical modeling of capillary flow in tubes of nonuniform cross section. *J. Colloid Interface Sci.* **2009**, *333*, 389−399.
(20) Lucas, R. Uber das zeitgesetz des kapillaren aufstiegs von flussigkeiten. *Kolloid Z.* **1918**, *23*, 15.
(21) Washburn, E. W. The dynamics of capillary flow. *Phys. Rev.* **1921**, *17*, 273−283.
(22) Theiß, W. Optical properties of porous silicon. *Surf. Sci. Rep.* **1997**, *29*, 91.
(23) Knittl, Z. *Optics of Thin Films (An Optical Multilayer Theory)*; John Wiley & Sons: New York, 1976.
(24) Landau, L. D.; Lifshitz, E. M. *Electrodynamics of Continuous Media*, 2nd ed.; Elsevier: New York, 1984; Vol. *8*.
(25) Alleborn, N.; Raszillier, H. Spreading and sorption of droplets on layered porous substrates. *J. Colloid Interface Sci.* **2004**, *280*, 449−464.
(26) Groisman, A.; Quake, S. R. A microfluidic rectifier: Anisotropic flow resistance at low reynolds numbers. *Phys. Rev. Lett.* **2004**, *92*, 094501.
(27) Tabeling, P. *Introduction to Microfluidics*; Oxford University Press: New York, 2005.